2014

Mutations in the Gene That Encodes the F-Actin Binding Protein Anillin Cause FSGS

R. A. Gbadegesin

G. Hall

A. Adeyemo

N. Hanke

I. Tossidou

See next page for additional authors

JASN

J Am Soc Nephrol. 2014 Sep; 25(9): 1991–2002.
Published online 2014 Mar 27. doi: 10.1681/ASN.2013090976
PMCID: PMC4147982
PMID: 24676636

Mutations in the Gene That Encodes the F-Actin Binding Protein Anillin Cause FSGS

Rasheed A. Gbadegesin,[*†] Gentzon Hall,[†‡] Adebowale Adeyemo,[§] Nils Hanke,[‖¶] Irini Tossidou,[‖] James Burchette,[**] Guanghong Wu,[†‡] Alison Homstad,[*†] Matthew A. Sparks,[‡] Jose Gomez,[‡] Ruiji Jiang,[*†] Andrea Alonso,[*†] Peter Lavin,[†‡‡] Peter Conlon,[‡‡] Ron Korstanje,[¶§§] M. Christine Stander,[‖‖] Ghaidan Shamsan,[‖‖] Moumita Barua,[¶¶] Robert Spurney,[‡] Pravin C. Singhal,[***] Jeffrey B. Kopp,[†††] Hermann Haller,[‖¶] David Howell,[**] Martin R. Pollak,[¶¶] Andrey S. Shaw,[‖‖] Mario Schiffer,[‖¶] and Michelle P. Winn[†‡]

Departments of [*]Pediatrics,
[‡]Medicine, and
[**]Pathology, and
[†]Center for Human Genetics, Duke University Medical Center, Durham, North Carolina;
[§]Center for Research on Genomics and Global Health, National Human Genome Research Institute, National Institutes of Health, Bethesda, Maryland;
[‖]Department of Nephrology, Hannover Medical School, Hannover, Germany;
[¶]Mount Desert Island Biological Laboratory, Salisbury Cove, Maine;
[††]Trinity Health Kidney Centre, Tallaght Hospital, Trinity College, Dublin, Ireland;
[‡‡]Department of Nephrology, Beaumont Hospital, Dublin, Ireland;
[§§]The Jackson Laboratory, Bar Harbor, Maine;
[‖‖]Howard Hughes Medical Institute, Department of Pathology and Immunology, Washington University School of Medicine, St. Louis, Missouri;
[¶¶]Division of Nephrology, Department of Medicine, Beth Israel Deaconess Medical Center, Boston, Massachusetts;
[***]Feinstein Institute for Medical Research, North Shore-LIJ Health System, Manhasset, New York; and
[†††]Kidney Disease Section, National Institute of Diabetes and Digestive and Kidney Diseases, National Institutes of Health, Bethesda, Maryland
[✉]Corresponding author.
Correspondence: Dr. Rasheed A. Gbadegesin, Department of Pediatrics, Duke University Medical Center, T-Level RM0909 CHC, Box 3959, Durham, NC 27710. Email: rasheed.gbadegesin@duke.edu

Received 2013 Sep 16; Accepted 2014 Jan 7.

Abstract

Go to:

FSGS is characterized by segmental scarring of the glomerulus and is a leading cause of kidney failure. Identification of genes causing FSGS has improved our understanding of disease mechanisms and points to defects in the glomerular epithelial cell, the podocyte, as a major factor in disease pathogenesis. Using a combination of genome-wide linkage studies and whole-exome sequencing in a kindred with familial FSGS, we identified a missense mutation *R431C* in *anillin* (*ANLN*), an F-actin binding cell cycle gene, as a cause of FSGS. We screened 250 additional families with FSGS and found another variant, *G618C*, that segregates with disease in a second family with FSGS. We demonstrate upregulation of anillin in podocytes in kidney biopsy specimens from individuals with FSGS and kidney samples from a murine model of HIV-1–associated nephropathy. Overexpression of *R431C* mutant ANLN in immortalized human podocytes results in enhanced podocyte motility. The mutant anillin displays reduced binding to the slit diaphragm–associated scaffold protein CD2AP. Knockdown of the ANLN gene in zebrafish morphants caused a loss of glomerular filtration barrier integrity, podocyte foot process effacement, and an edematous

phenotype. Collectively, these findings suggest that anillin is important in maintaining the integrity of the podocyte actin cytoskeleton.

FSGS is a clinicopathologic entity that is characterized by nephrotic syndrome (NS), focally sclerotic glomeruli, and effacement of podocyte foot processes and is a common cause of ESRD.[1] The pathogenesis of FSGS has not been completely elucidated; however, recent advances in molecular genetics have provided evidence that disruption of podocyte structure and function is central to its pathogenesis. The highly specialized apparatus of the glomerular filtration barrier (GFB) is composed of the podocyte and slit diaphragm, the glomerular basement membrane, and specialized fenestrated endothelium. The podocyte and slit diaphragm play a central role in maintaining the structural and functional integrity of the GFB. This is evidenced by the number of genetic mutations found in familial FSGS and NS; many of these gene products contribute to signaling at the podocyte slit diaphragm or localize to the podocyte cytoskeleton.[2–8] However, the entire repertoire of genes and proteins that are important in maintaining the functional integrity of the GFB remains unknown. It is estimated that >90% of the genetic causes of hereditary FSGS and NS remain unknown[9]; thus, the study of large kindreds remains an invaluable tool for unraveling the complexity of the molecular interactions that are responsible for maintaining the integrity of the podocyte and GFB.

We identified a pedigree from the United States with autosomal dominant (AD) FSGS. Linkage analysis was carried out and we obtained suggestive multipoint logarithm of odds (LOD) scores of 1.7, 1.7, and 1.8 on chromosomes 2p, 5p, and 7p respectively. Whole-exome sequencing identified a deleterious heterozygous mutation *R431C* in *ANLN,* the gene encoding the F-actin binding protein anillin. We found another variant *G618C* that segregates with disease in a second family with FSGS. Anillin is important in cytokinesis and it interacts with key proteins such as CD2AP and mDia2 during cell division.[10–13] In addition, it regulates cell growth by its interaction with the promigratory and prosurvival phosphoinositide 3 kinase/AKT (protein kinase B) pathway.[10–13] Overexpression of the mutant anillin in immortalized human podocytes causes increased podocyte motility compared with wild-type overexpression. In contrast with intact anillin, the mutant displays a significantly reduced binding affinity to CD2AP. These findings reemphasize the importance of podocyte cell integrity, cell survival pathways, and cell migration in the pathogenesis of FSGS.

Results

Go to:

Clinical Data and Linkage Analyses

Family 6562 is a 26-member kindred from the United States known to date back four generations. There are nine affected individuals in this family. Both male and female individuals are affected in at least four generations and there is male-to-male transmission, consistent with an AD inheritance pattern (Figure 1A). A summary of clinical findings in affected individuals is shown in Table 1. Briefly, the age of onset of ESRD occurred between 35 and 75 years. Five people received kidney transplants and there was no recurrence of FSGS in the renal allograft. Figure 1B is a representative sample of kidney histology from one of the affected individuals. Disease-causing mutations were not found in known FSGS genes in affected individuals.[3–7] We performed genome-wide linkage analysis in this family and obtained multipoint LOD scores of 1.7 on chromosomes 2p and 5p, and 1.8 on chromosome 7p (Figure 1C). The chromosome 2p, 5p, and 7p regions span physical distances of 33.4, 4.0, and 22.1 Mb, respectively.

Whole Exome and Targeted Podocyte Exome Sequencing

The DNA from the proband was subjected to whole exome sequencing using the Illumina TruSeq platform. On average, the genomic coverage was 52×. After excluding variants with minor allele frequencies >1%, 1179 novel variants were identified. The following parameters were used to determine

the disease-causing mutation: (*1*) all variants found in our database of 1600 normal control chromosomes were removed, (*2*) known variants that were in dbSNP (http://www-ncbi-nlm-nih-gov.medproxy.hofstra.edu/projects/SNP/) and the 1000 Genomes Project (http://www.1000genomes.org/) were removed, (*3*) all synonymous variants were removed, and (*4*) all intronic variants were removed, except splice site variants and variants in promoter regions. DNA from the same individual was sequenced using a custom exome chip with 2400 genes that are expressed in human podocytes and was compared with the whole-exome sequencing results. After applying these parameters, there were 146 potential disease-causing variants from the whole exome data and 62 from the targeted podocyte exome data (with 20 variants common to both approaches). Six variants in the peaks on chromosomes 2p, 5p, and 7p were identified and confirmed by Sanger sequencing (Table 2). The *ANLN* gene is in the chromosome 7p peak (Figure 1C). A nonsynonymous heterozygous change in exon 7 c. *1291C >T R431C* in anillin (*ANLN*) was identified in all affected individuals (Figure 1D, top and bottom chromatograms show an affected individual and a control individual, respectively). Of the six variants in the chromosome 2p, 5p, and 7p peaks, only the *ANLN R431C* variant segregated with the disease in the family. The variant was not found in >1600 control chromosomes. This is an ample number of controls for a rare Mendelian disease; a minimum of 350 controls are needed for 95% power to detect 1% polymorphism frequency.[14] The mutated residue is conserved in evolution to zebrafish (Figure 1E). *In silico* modeling showed that the variant is damaging, with a polyphen score of 0.91.[15,16] The list of potentially pathogenic variants with a minor allele frequency <1% in chromosome 2p, 5p, and 7p loci is shown in Supplemental Table 1. We screened 100 more families from our cohort and did not find any disease-causing variant, other known and novel *ANLN* variants found in this cohort are listed in Supplemental Table 2. We screened 150 more families from another cohort (MRP) and found another variant exon 10 c. 1852 G>T *G618C* that segregates with disease in another family. The *G618C* variant is predicted to be damaging, with a polyphen score of 0.99. The variant is absent in the 1000 Genomes Project database. The family with the *G618C* variant has three affected individuals in two generations. A DNA sample was available from FG-JG1, FG-JG10, FG-JG12, FG-JG13, and FG-JG14 (Supplemental Figure 1). The pedigree and results of mutation analysis are shown in Supplemental Figure 1.

Anillin Is Upregulated in Human and Murine FSGS

Real-time RT-PCR was performed on RNA isolated from kidney, brain, heart, lung, liver, and spleen from three wild-type 129 Sv/Ev mice. ANLN is ubiquitously expressed in all organs, with the highest level of expression in the heart (Figure 2A). Immunohistochemical staining of normal human kidney biopsy tissue using rabbit anti-human anillin polyclonal antibody showed that anillin is widely expressed in tubules but sparsely expressed in a nuclear pattern in the glomerulus, suggesting that anillin is minimally expressed in normal podocytes (Figure 2B). This is consistent with a previous observation that anillin is not expressed in terminally differentiated cells that have exited the cell cycle.[17] In renal biopsy specimens from humans with idiopathic FSGS, expression of anillin was significantly upregulated and synaptopodin expression was downregulated in areas of the glomerulus that stain strongly for anillin (Figure 2C).

To further delineate the cell population that expresses anillin in the glomerulus, we obtained kidney tissue from rtTA/Vpr (HIVAN VPR) mice,[18] a model that is characterized by abnormal podocyte proliferation and collapsing FSGS. We performed standard double immunostaining for WT1, a key podocyte gene, and anillin in wild-type and HIVAN VPR mice (Figure 2, D–K). Anillin expression is increased in the glomerulus of HIVAN mice (Figure 2J) compared with wild-type mice (Figure 2F). Anillin colocalizes with WT1 using confocal microscopy in the glomerulus of HIVAN mice, suggesting that the cells expressing anillin are podocytes (Figure 2K).

Overexpression of R431C ANLN Results in Aberrant Binding to CD2AP

Anillin associates with CD2AP and Cindr (CIN85), the single *Drosophila melanogaster* ortholog of CD2AP.[19,20] CD2AP is an important cytoskeletal protein involved in the cellular adhesion and cell migration through interactions with various actin regulatory proteins such as CAPZ, cortactin, Rac1, and ANLN.[19,20] In podocytes, CD2AP has an additional important role as an adaptor molecule linking the slit diaphragm protein nephrin to the actin cytoskeleton.[19,20] Because CD2AP is an established anillin binding partner, we posit that the R431C mutation may alter the binding of anillin to CD2AP. To evaluate this, we performed standard immunofluorescence staining on undifferentiated podocyte cell lines and determined that endogenous CD2AP targeted to anillin at podocyte plasma membrane blebs (Figure 3A). Because peripheral membrane blebs have been shown to be sites of dynamic actin polymerization/depolymerization involved in cell motility, this result suggests that the CD2AP/anillin interaction may be an important actin regulatory component underlying the mechanics of podocyte motility.[21] To understand the effect of the R431C mutation on anillin and CD2AP interaction, we performed standard immunoprecipitation experiments with CD2AP in the HEK-293 cell line. Overexpression of the $ANLN_{R431C}$ mutant results in reduced and defective binding with CD2AP compared with the wild type ($P<0.002$) (Figure 3, B and C). These results indicate that the identified disease mutation could alter the known functions of CD2AP in podocytes.

Overexpression of Wild-Type and Mutant *ANLN* Causes Aberrant Podocyte Migration

Anillin was previously shown to play a vital role in the promigration and prosurvival phosphoinositide 3-kinase/AKT pathway.[10,12] We explored the role of defective anillin on podocyte migration. First, immortalized undifferentiated cultured human podocytes were stably transfected with tGFP empty vector, tGFP-tagged wild-type ($ANLN_{WT}$), or mutant ($ANLN_{R431C}$) anillin constructs using the lentivirus gene delivery system. We demonstrated 95% transfection efficiency by FACS analyses and also by Western blotting. We performed standard wound healing assays as a surrogate of podocyte motility on both the wild type and mutant overexpression line.[22] The mutant cell line ($ANLN_{R431C}$) demonstrated increased cell motility compared with the overexpression $ANLN_{WT}$ (Figure 4). These findings suggest that anillin may play a significant role in podocyte cell migration.

Anln Knockdown in Zebrafish Causes Disruption of the GFB

As a test for the *in vivo* relevance of anillin function, we performed morpholino knockdown experiments in zebrafish. A splice-donor morpholino specific for the anillin zebrafish ortholog and a scrambled control were injected and the development of edema was monitored for up to 120 hours postfertilization. The fish were rated as normal (phenotype I) or having mild edema (phenotype II), severe edema (phenotype III), or very severe edema (phenotype IV). The majority of the *anln* morpholino-treated fish developed a severe edematous phenotype (phenotypes III and IV) in contrast with control morpholino-injected fish and wild-type fish from the same clutches with >90% normal phenotypes (phenotype I) (Figure 5A). Anillin-knockdown zebrafish and control injected zebrafish were then injected with FITC-labeled 70-kD dextran to demonstrate that edema was caused by a systemic loss of high molecular mass proteins. Systemic fluorescence activity in the retinal vessels of the fish was monitored, utilizing an assay system that we have used in the past to verify proteinuria development.[23,24] We detected a significant loss of 70-kD dextran especially in the severe phenotypes of anillin-knockdown fish (Figure 5B). To verify these observations in a second model system, we used the Tg (l-fabp:DBP-EGFP) model system.[25] This transgenic fish produces significant amounts of a circulating vitamin D–binding protein (DBP) fused to enhanced green fluorescent protein (EGFP) with a molecular mass of approximately 64 kD. The transgene expression is driven by a fatty acid binding protein promoter that becomes active 72 hours postfertilization. When we compared accumulation of this endogenously produced marker in control and anillin morpholino-injected fish, we documented a similar systemic loss of this high molecular mass protein in severely but also in mildly affected anillin-knockdown fish (Figure 5C). In addition, dot blot

analysis of the fish water revealed that the anillin-knockdown fish had increased DBP-EGFP excretion in water compared with the control morpholino and the wild-type (Figure 5C). Finally, transmission electron microscopy (TEM) revealed fusion and almost complete effacement of the podocyte foot processes and disorganization of the GFB in the anillin-knockdown fish compared with the control (Figure 5D). The structure of the glomerular basement membrane and the fenestration of the endothelium appeared normal in the control fish. These data indicate a significant loss of high molecular mass proteins from the circulation in the absence of functional anillin in this *in vivo* proteinuria model and also demonstrated disruption of the GFB specifically with a clear podocyte phenotype on TEM.

Discussion

Go to:

Here we report a new cause of hereditary FSGS using a unique strategy for the identification of disease-causing mutations in an AD FSGS pedigree. Our strategy utilizes genome-wide linkage analysis and dual sequencing approaches of the whole exome and a custom-designed capture that was targeted toward genes that are known to be enriched in the podocyte, the glomerular visceral epithelial cell that is believed to be central to the pathogenesis of FSGS. With rapid advances in molecular genetics and cell biology, this method will have wide applicability to diseases in which specific cells or pathways are known to be central to disease evolution.

We discovered a novel mutation R431C in ANLN, the only gene variant that segregated in affected individuals in the family under study. The gene encodes for anillin, an F-actin binding protein that is enriched in the cytoskeleton. Anillin is a 124-kD protein with a nuclear domain, an F-actin binding domain, a coiled-coil domain, and a pleckstrin homology domain, among others.[17,26] It functions as a scaffold protein that links RhoA and mDia2 (mouse formin 2) with actin and myosin in the cleavage furrows that is formed during cytokinesis and cellularization; in addition, it binds and bundles F-actin *in vitro*.[10,13,26] The R431C mutation is in the F-actin binding domain of the protein, suggesting that the change may affect organization of the actin cytoskeleton.

We sequenced the entire ANLN gene in at least 250 families with FSGS and found an additional variant G618C that segregate with disease in another family with FSGS. The low frequency of pathogenic ANLN variants may be because anillin is essential for cell division and it participates in pathways that are critical during development.[12,13] It is, however, possible that some hypomorphic alleles in ANLN may be susceptibility factors for FSGS. Additional datasets will need to be examined for ANLN mutations to determine the actual prevalence. At the mRNA level, anillin is ubiquitously expressed in all organs, with the highest level of expression in the heart.

We showed expression of anillin in tubules from normal human kidney biopsy samples; however, there was weak expression in the glomerulus and the podocyte. This finding is not surprising because tubules are actively dividing cells, whereas adult podocytes are thought to be terminally differentiated. This finding is consistent with the observation of Field and Alberts that anillin is not expressed in cells that have exited the cell cycle.[17] Interestingly, anillin was upregulated in the glomeruli of kidney biopsies from individuals with idiopathic FSGS. One possible explanation is that aberrant reentry of podocytes into the cell cycle and pathologic dedifferentiation may be one of the mechanisms by which defective anillin may cause FSGS. It is interesting to note that a recent study demonstrated the ability of adult podocytes to reversibly enter the cell cycle in HIV-associated FSGS.[27] To determine whether the cells that are expressing anillin in the human glomerulus are podocytes, we obtained kidney tissue from a murine model of collapsing FSGS (VPR HIVAN mice).[18] Similar to what we observed in human FSGS, we showed upregulation of anillin in the glomerulus. In addition, anillin colocalized with WT1, suggesting that the cells expressing anillin are likely to be abnormal podocytes.

To investigate the mechanisms that contribute to the development of FSGS in patients expressing R431C anillin, we explored the role of CD2AP binding to normal and mutant anillin. The rationale for these

experiments was based on the observation that anillin associates with Cindr, the single ortholog of CD2AP/CIN85 in *D. melanogaster*.[19,28] CD2AP is also an important signaling molecule in podocytes linking the slit diaphragm protein nephrin to the actin cytoskeleton and promoting Akt-dependent signaling.[20] In addition, CD2AP binds actin regulating proteins such as CAPZ and cortactin as well as Rac1; CD2AP is therefore an important cellular protein involved in regulating podocyte migration.[29] Mice lacking CD2AP develop NS, and mutations predicted to ablate CD2AP expression in humans are associated with FSGS.[2] Similar to CD2AP, anilin serves as a scaffolding protein and binds F-actin, active myosin II, septins, and the small GTPase Rho.[12] In this study, we showed that the wild-type anillin also binds CD2AP and that this binding is impaired by the R431C mutation. This aberrant binding promoted increased podocyte motility in the mutant cell line. Because abnormal podocyte motility has been associated with both loss of GFB integrity and foot process effacement,[30,31] these data are consistent with the notion that anillin plays a key role in regulating actin cytoskeletal dynamics. These actin regulatory mechanisms are disrupted by the mutant anillin, which, in turn, may promote the development of FSGS.[19,20,29]

To determine if anillin played a role in regulating GFB integrity *in vivo*, we generated a zebrafish with a knockdown of the anln gene. The knockdown zebrafish developed proteinuria, food process effacement, and an edematous phenotype. Although further studies will be necessary to clarify the functional effect of mutant anillin *in vivo*, these data are consistent with the notion that anillin plays a key role in regulating the integrity of the GFB and not necessarily the mechanisms by which the R431C may cause FSGS.

In summary, we used combined linkage analysis, whole exome sequencing and a podocyte targeted exome sequencing approach to identify a mutation in ANLN as a cause of hereditary FSGS. The mutation segregates in the family and was absent from >1600 control chromosomes. Immunohistochemistry, immunofluorescence, and confocal studies in kidney biopsy tissue from individuals with FSGS and HIVAN mice showed aberrant overexpression of anillin compared with normal kidney. Mutant ANLN exhibited reduced binding to adaptor protein CD2AP and promoted aberrant podocyte migration. Anln zebrafish morphants developed edema, foot process effacement, and a loss of GFB integrity similar to humans with FSGS. Our findings suggest that anillin is important in regulating podocyte actin cytoskeletal dynamics and implicates anillin mutations in the pathogenesis of FSGS.

Concise Methods

Go to:

Case Ascertainment

This study was approved by the institutional review boards of Duke University Medical Center (Durham, NC) and Brigham and Women's Hospital (Boston, MA). Informed and written consent and assent from minors were obtained from all human participants in this study. All animal protocols were approved by the National Institutes of Health (NIH) National Institute of Diabetes and Digestive and Kidney Diseases and the Mount Desert Island Biologic Laboratory (MDIBL) Animal Care and Use Committee. Inclusion criteria and determination of affection status are as previously reported.[32] We excluded mutations in known FSGS genes (*NPHS1, NPHS2, PLCE1, ACTN4, TRPC6,* and *INF2)* in all of the affected individuals.

Linkage Analyses

A genome-wide linkage scan was performed using the Illumina Infinium II HumanLinkage-24 genotyping beadchip assay (Illumina, Inc., San Diego, CA). Genotyping was performed on the 12 individuals from the family comprising six affected individuals and six unaffected individuals. Two-point and multipoint LOD scores were calculated for all 5000 single nucleotide polymorphism markers. A rare dominant model was assumed. A conservative "affecteds-only" analysis was performed to ensure that results obtained were not because of asymptomatic individuals.

Whole Exome Sequencing and Podocyte Exome Sequencing

Whole exome sequencing was performed on the proband using standard protocol. We used the Agilent All Exon 50MB kit and sequenced to 78.3×coverage using one lane of a HiSEquation 2000 sequencer. Reads were aligned to the Human Reference genome (HG 18) using BWA software.[33] Any homozygous variants with <10×coverage were also Sanger sequenced to eliminate false negative results. Single nucleotide variants were called using SAMtools.[34] The variants were annotated to Ensembl 50_36l using SequenceVariantAnalyzer and were analyzed using ATAV software (http://www.duke.edu/~minhe/atav/).[33,35]

For podocyte exome sequencing, one of the authors (A.S.) designed an exon capture sequence chip containing 2400 genes that are enriched in the podocyte. The gene list was derived from microarrays of human and mouse podocyte cell lines and glomeruli from human kidney biopsies. All known FSGS or CKD genes identified in genome-wide association studies were added to the list. The MetaCore function of GeneGO (http://GeneGo.com) was used to place all of these genes into pathways.

Sanger Sequencing

Potential disease-causing variants identified by both whole exome and whole podocyte exome chips were confirmed by Sanger sequencing. Exon primer sequences and cDNA are listed in Supplemental Tables 3 and 4. All sequences were analyzed with Sequencher software (Gene Codes Corp., Ann Arbor, MI).

In Silico Prediction of the Effect of Amino Acid Substitution

The *R431C* and the *G618C* variants in the *ANLN* gene were entered into SIFT and PolyPhen-2 software to examine the predicted damaging effect of the amino acid substitution to the function of *ANLN*. PolyPhen-2 calculates a naïve Bayes posterior probability that any mutation is damaging and this is represented with a score ranging from 0 to 1.[15]

mRNA Extraction from Tissues

Experimental studies were conducted within the first three to four passages of the podocyte subculture. Total RNA was manually extracted from whole kidney, brain, heart, liver, lung, and spleen tissues from wild-type mice using an RNeasy Mini kit (Qiagen, Valencia, CA). Tissue was stabilized in RNAlater solution (Ambion Inc., Austin, TX) immediately after mice were euthanized. Subsequently, 0.5 μg of total RNA was reverse transcribed into cDNA utilizing the RT system (Promega, Madison, WI) with oligo(dT) primers, according to the manufacturer's protocol. Relative expression of the target genes was analyzed by normalizing to the housekeeping gene *β-Actin* (primer sequences for ANLN and ANLN cDNA are provided in Supplemental Tables 2 and 3).

Immunohistochemistry Human Kidney Biopsy

Single-label immunohistochemistry was performed on formalin-fixed, paraffin-embedded tissue sections using mouse monoclonal synaptopodin antibody clone G1D4 at 1:80 dilution (Acris Antibodies, San Diego, CA) and anillin rabbit polyclonal antibody at 1:100 and 1:200 dilution (Bethyl Laboratories, Inc., Montgomery, TX). Detection of the bound antibody was accomplished with the use of a Bond Refine horseradish peroxidase–labeled detection system (Leica Microsystems). The bound immune complex was visualized with the on-line application of diaminobenzidine and subsequently counterstained with hematoxylin. Completed slides were dehydrated with alcohol, cleared with xylene, and coverslipped with a permanent mounting media. Double-stain immunohistochemistry was manually performed on paraffin-embedded tissue sections by preparing antibody cocktails of synaptopodin (1:80 dilution) and anillin (1:100 dilution). After paraffin removal, clearing, and quenching of endogenous peroxidase activity and hydration, tissue sections were pretreated for 20 minutes in 99°C Tris/EDTA epitope retrieval solution.

Anillin/synaptopodin antibody cocktails were applied to the tissue sections and incubated for 60 minutes. Detection of the bound antibodies was accomplished by applying Mach 2 Kit 1 or Mach 2 Kit 2 (Biocare Medical, Concord CA). Comparative color combinations of tissue sections for anillin/synaptopodin double-stain immunohistochemistry were performed. The labeled antibody complex was detected by sequential application of chromogenic substrates diaminobenzidine and Fast Red. Tissue sections were counterstained with hematoxylin and air dried before coverslipping with a permanent mounting medium.

Immunofluorescence and Confocal Microscopy of Kidney Tissues from HIVAN VPR Mice

rtTA/Vpr (VPR HIVAN) mice were obtained by crossing podocin/rtTA mice (constitutively expresses the rtTA, which is a fusion protein composed of the TetR repressor and the VP16 transactivation domain from the podocin promoter) with tetop/Vpr mice (TRE-regulated Vpr gene). HIVAN mice were provided doxycycline in their drinking water for 6 weeks to induce the expression of the podocyte-specific Vpr gene, whereas wild-type control mice did not receive doxycycline. For immunofluorescence, mice were perfused with 10 ml of PBS and then 4 ml of 4% paraformaldehyde. Kidneys were removed and soaked in 4% paraformaldehyde overnight and then placed in 30% sucrose/PBS for 4 hours at 4°C. Kidneys were frozen in optimal cutting temperature medium at −80°C. Kidney sections were made at 8 μm. Excess water was removed from tissue by soaking in 100% ETOH for 10 minutes, and then tissue was rehydrated with graded ETOH baths (95%–70% ETOH) and then water and PBS. Antigen retrieval was performed with 10 mM of citrate buffer (pH 6.0) in a pressure cooker for 20 minutes. Tissue was blocked with 5% factor V BSA/PBS for 1 hour, and sections were incubated with primary antibodies diluted in 5% factor V BSA/PBS overnight at 4°C. Slides subsequently were washed in PBS and incubated with secondary fluorochrome-conjugated antibodies for 45 minutes at room temperature. Slides were coverslipped using Fluoromount-G containing 2 mg/ml 4′,6-diamidino-2-phenylindole (Sigma-Aldrich, St. Louis, MO). The following primary antibodies were used: goat anti-ANILLIN (1:100 dilution, EB06104; Everest Biotech, Ramona, CA), and rabbit anti-WT-1 (1:100 dilution, sc-192; Santa Cruz Biotechnology, Santa Cruz, CA). The following secondary antibodies were used in 1:500 dilutions for 45 minutes at room temperature: Alexa 594 donkey anti-rabbit IgG (A-21207) and Alexa 488 donkey anti-goat IgG (A-11055) were purchased from Invitrogen. Immunofluorescence staining was visualized and photographed using a Zeiss 510 Inverted Confocal Microscope (Carl Zeiss, Jena, Germany).

Immunofluorescence of Podocyte Cell Lines

Immortalized human podocytes were cultured on collagen I–coated coverslips (BD Biosciences, San Jose, CA) and treated as indicated. Cells were then fixed and washed with PBS and blocked with buffer containing 5% goat serum before incubation with rabbit polyclonal Anillin antibody (Bethyl Laboratories), and mouse monoclonal CD2AP antibody (Santa Cruz Biotechnology). Cells were washed with PBS and secondary Alexa Fluor 488 antibody was applied (Invitrogen) at a concentration of 1:1000 for 1 hour at room temperature. Cells were washed with PBS before addition of 4′,6-diamidino-2-phenylindole stain at a concentration of 1:10,000 diluted in PBS. Podocyte immunofluorescence imaging was performed using a Zeiss AxioImager and the MetaMorph Bioimaging Software.

For lentivirus construction and cell transduction with *ANLN*, standard molecular cloning methods were used to replace the ubiquitin-EGFP of FUGW with CMV turboGFP (tGFP vector control), CMV turbo-WT-ANLN (tGFP-ANLN$_{WT}$), and CMV turboGFP-mutant-ANLN (tGFP-ANLN$_{R431C}$).[36] Lentivirus was made by transfecting 6×106 293FT (Invitrogen) cells with 5 μg VSVg, 15 μg Δ8.9, and 20 μg promoter-reporter plasmid using Lipofectamine 2000. After 72 hours, supernatant was harvested, filtered at 0.45 μm, and pelleted by ultracentrifugation at 26,000 rpm for 2 hours at 4°C. After resuspension in HBSS, lentivirus was stored at −80°C. Conditionally immortalized human podocytes were then transduced with either tGFP vector control, tGFP-ANLN$_{WT}$, or tGFP-ANLN$_{R431C}$ lentiviruses for 24 hours in RPMI 1640

media. Cells were allowed to grow to 95% confluence before harvest and sorting by flow cytometry. tGFP-expressing cells were then plated in growth media and returned to standard growth permissive conditions.

Wound Healing Assays

Conditionally immortalized human podocytes were transduced with either tGFP vector control, tGFP-$ANLN_{WT}$, or tGFP-$ANLN_{R431C}$ lentiviruses for 24 hours and cells were allowed to grow to confluence. Cell monolayers were washed and scratch wounds were applied using a 1000-μl pipet tip. Podocytes were imaged using an EVOS microscope at time 0 immediately after wound creation. Cells were then returned to growth restrictive conditions for 24 hours before final imaging of wound healing.

Immunoblotting and Immunoprecipitation

HEK-293T cells were transfected with plasmids expressing flag epitope-tagged human CD2AP DNA and wild-type anillin or mutant anillin DNA. The cells were then washed carefully with ice-cold PBS on ice. For lysis, 900 μl RIPA buffer (50 mM TrisHCl, pH 7.5, 200 mM NaCl, 1 mM EDTA, 1 mM EGTA, 1% Triton, and 0.25% deoxycholate plus protease inhibitors) was added to cells. The lysate was incubated for 15 minutes on ice and centrifuged at 14,000 rpm for 15 minutes at 4°C. Fifty-microliter flag-beads (50% slurry in Triton buffer; Sigma-Aldrich) were added to the supernatant and rotated overhead at 4°C for 1 hour (up to overnight). After that, the beads were centrifuged at 3000 rpm for 1 minute at 4°C and washed with RIPA buffer five times. Proteins were eluted by boiling the beads in Laemmli buffer and separated by SDS-PAGE.

Zebrafish Stocks and Injections

Zebrafish (AB) were grown and mated at 28.5°C, and embryos were kept and handled in standard E3 solution as previously described.[37] Morpholinos were injected in fertilized eggs in the one- to four-cell stage using a Nanoject II injection device (Drummond Scientific, Broomall, PA). The following morpholinos were designed and ordered from GeneTools (Philomath, OR): control, 5′-CCTCTTACCTCAGTTACAATTTATA-3′; and Anillin, 5′-GGCCCCTGAAAACAGTTGTATAGAT-3′. Morpholino injections were carried out with concentrations ranging from 50 to 100 μM, with an injection volume of 4.6 nl in injection buffer (100 mM KCl, 0.1% phenol red). Embryos were monitored for the development of phenotype until 120 hours postfertilization. The phenotype was scored from one to four, relative to the amount of edema present.

Eye Assays

Two types of eye assays were performed to assess proteinuria. At 50–55 hours after morpholino injection, remaining chorions were manually removed from all embryos. For one group, cardinal vein injections were performed as described by Hentschel *et al*.[23] Briefly, 4.6 μl of FITC-labeled 70-kD dextran (Molecular Probes, Eugene, OR) was injected into the cardiac venous sinus. For this injection, zebrafish were anesthetized with a 1:20–1:100 dilution of 4 mg/ml Tricaine (MESAB: ethyl-*m*-aminobenzoate methanesulfonate, 1% Na_2HPO_4, pH 7.0; Sigma-Aldrich) and positioned on their backs in a 1% agarose injection mold. After the injection, fish were returned to egg water, where they quickly regained motility.

A second assay was performed measuring endogenous fluorescence intensity of retinal blood vessels in Tg (l-fabp:DBP-EGFP) zebrafish (gift from J. Xie and B. Anand-Apte, Cleveland, OH)[25] at 96, 120, and 144 hours after morpholino injection. These animal protocols were approved by the MDIBL Animal Care Committee.

Image Analyses

For eye assay measurements, zebrafish larvae were transferred into individual wells of a 96-well plate (Thermo Fisher Scientific, Pittsburgh, PA). Fish were anesthetized with Tricane and sequential images of live fish were generated using a Zeiss inverted microscope (Axiovert 200) connected to an AxioCam MRm charge-coupled device camera, and images were taken with fixed exposure times and gain using the Axio Vision release 4.5 SP1 software package. The maximum fluorescence intensities of images of the pupil of the fish were measured using the NIH ImageJ application and are reported in relative units of brightness.

Dot Blot Analyses of Fish Water

For dot blot analysis of fish water, 150 μM of Anillin and control morpholinos was injected into Tg(Fabp:DBP-eGFP) male crossed with wild-type female embryos. Fish were transferred to 48-well plates individually (one fish per well) with 500 μl of embryo raising medium at 72 hours and kept at 28°C until 168 hours. Fish were graded for phenotype development, removed from the wells, and the fish water was stored at −20°C. Only fish water from fish with a heartbeat at 168 hours was used for dot blot analysis. For the dot blot procedure, 100 μl of fish water from four fish was pooled and blotted on a nitrocellulose membrane. Immunoblotting was performed using anti-GFP (Abcam, Inc.; ab290) 1:2000/anti-rabbit 1:5000 in PBS/5% nonfat dry milk. Total EGFP protein was extracted from an individual fish and was used as a positive control on the dot blot in % dilutions as indicated in Figure 5C. Epon embedding of zebrafish embryos was performed following standard procedures, and TEM of the zebrafish pronephros was performed.

Statistical Analyses

Continuous variables that were normally distributed were expressed as the mean±SD. Differences between two groups were compared using the *t* test. Categorical variables were compared by the chi-squared test and Fisher's exact test where indicated. A P value <0.05 was considered statistically significant.

Disclosures

Go to:

None.

Supplementary Material

Go to:

Supplemental Data:

Acknowledgments

Go to:

We thank Lynne Staggs and Patricia Schroder (MDIBL) for technical assistance with the zebrafish experiments, Sophie Paschke for zebrafish artwork, and Dr. Donald Houghton for his help in interpretation of renal histology and constructive review of the manuscript. We also thank Dr. Elizabeth T. Cirulli, Dr. David B. Goldstein, Dr. Kevin V. Shianna, and the personnel of the Center for Human Genome Variation for assistance with sequencing. In addition, we acknowledge the following individuals for the contributions of control samples: Dr. James Burke, Dr. Christine Hulette, Dr. Kathleen Welsh-Bohmer, Dr. Francis J. McMahon, Nirmala Akula, Dr. Julie Hoover-Fong, Dr. Nara L. Sobreira, Dr. David Valle, Dr. M. Chiara Manzini, Dr. Annapurna Poduri, Dr. Nicole Calakos, Mr. David H. Murdock and The MURDOCK Study Community Registry and Biorepository, Dr. Joseph McEvoy, Dr. Anna Need, Mr. Jordan Silver, Ms. Marlyne Silver, Dr. Eli J. Holtzman, Dr. Gianpiero Cavalleri, Dr. Norman Delanty, Dr. Chantal Depondt, Dr. Sanjay Sisodiya, Dr. William B. Gallentine, Dr. Erin L. Heinzen, Dr. Aatif M. Husain, Ms. Kristen N. Linney, Dr. Mohamad A. Mikati, Dr. Rodney A. Radtke, Dr. Saurabh R. Sinha, Ms. Nicole M. Walley, Dr. Deborah Koltai Attix, Ms. Vicki Dixon, Ms. Jill McEvoy, Dr. Vandana Shashi, Dr. Patricia Lugar, Dr. William L. Lowe, Dr. Scott M. Palmer, Dr. Doug Marchuk, Dr. Deborah Levy, Dr. Zvi Farfel, Dr. Doron Lancet, Dr. Elon Pras, Dr. Yong-Hui Jiang, Dr. Qian Zhao, Dr. Joshua Milner, Dr. Demetre Daskalakis, Mr.

Arthur Holden, Dr. Elijah Behr, Dr. Robert H. Brown Jr., Dr. Sarah Kerns, and Dr. Harriet Oster. Finally, we thank the personnel of the Center for Human Genetics core facilities and most importantly the family members of the Duke FSGS project. This study was funded by grants from the NIH National Institute of Diabetes and Digestive and Kidney Diseases (NIDDK) (K08-DK082495 and 1R56-DK098135-01 to R.G.; 5R01-DK074748-06 to M.P.W.). This research was supported in part by funding from the NIH Division of Intramural Research and the National Institute of Allergy and Infectious Diseases (NIAID). The sequenced controls used for this study were funded in part by the American Recovery and Reinvestment Act (1RC2-NS070342-01), the Joseph and Kathleen Bryan Alzheimer's Disease Research Center and the National Institute on Aging (P30-AG028377), the National Institute of Mental Health (RC2-MH089915), and the NIAID (1R56-AI098588-01A1). R.G. is supported by grants from the NephCure Foundation as well as the Doris Duke Clinical Scientist Development Award, and acknowledges that this work was supported by a grant from the Doris Duke Charitable Foundation (2009033). M.P.W. is a recipient of the DukeMed Scholars program. M.S. is supported by the German Research Foundation (SCHI587/4,6). N.H. is supported by an MDIBL New Investigator Award. A.S.S. is supported by the Howard Hughes Medical Institute and the NIDDK.

Footnotes

Go to:

Published online ahead of print. Publication date available at www.jasn.org.

This article contains supplemental material online at http://jasn.asnjournals.org.medproxy.hofstra.edu/lookup/suppl/doi:10.1681/ASN.2013090976/-/DCSupplemental.

References

Go to:

1. US Renal Data Service : USRDS 2012 Annual Data Report: Atlas of Chronic Kidney Disease and End-Stage Renal Disease in the United States, Bethesda, MD, National Institutes of Health, National Institute of Diabetes and Digestive and Kidney Diseases, 2012

2. Shih NY, Li J, Karpitskii V, Nguyen A, Dustin ML, Kanagawa O, Miner JH, Shaw AS: Congenital nephrotic syndrome in mice lacking CD2-associated protein. Science 286: 312–315, 1999 [PubMed: 10514378]

3. Boute N, Gribouval O, Roselli S, Benessy F, Lee H, Fuchshuber A, Dahan K, Gubler MC, Niaudet P, Antignac C: NPHS2, encoding the glomerular protein podocin, is mutated in autosomal recessive steroid-resistant nephrotic syndrome. Nat Genet 24: 349–354, 2000 [PubMed: 10742096]

4. Kaplan JM, Kim SH, North KN, Rennke H, Correia LA, Tong HQ, Mathis BJ, Rodríguez-Pérez JC, Allen PG, Beggs AH, Pollak MR: Mutations in ACTN4, encoding alpha-actinin-4, cause familial focal segmental glomerulosclerosis. Nat Genet 24: 251–256, 2000 [PubMed: 10700177]

5. Winn MP, Conlon PJ, Lynn KL, Farrington MK, Creazzo T, Hawkins AF, Daskalakis N, Kwan SY, Ebersviller S, Burchette JL, Pericak-Vance MA, Howell DN, Vance JM, Rosenberg PB: A mutation in the TRPC6 cation channel causes familial focal segmental glomerulosclerosis. Science 308: 1801–1804, 2005 [PubMed: 15879175]

6. Hinkes B, Wiggins RC, Gbadegesin R, Vlangos CN, Seelow D, Nürnberg G, Garg P, Verma R, Chaib H, Hoskins BE, Ashraf S, Becker C, Hennies HC, Goyal M, Wharram BL, Schachter AD, Mudumana S, Drummond I, Kerjaschki D, Waldherr R, Dietrich A, Ozaltin F, Bakkaloglu A, Cleper R, Basel-Vanagaite L, Pohl M, Griebel M, Tsygin AN, Soylu A, Müller D, Sorli CS, Bunney TD, Katan M, Liu J, Attanasio M, O'toole JF, Hasselbacher K, Mucha B, Otto EA, Airik R, Kispert A, Kelley GG, Smrcka AV, Gudermann T, Holzman LB, Nürnberg P, Hildebrandt F: Positional cloning uncovers mutations in PLCE1 responsible for a nephrotic syndrome variant that may be reversible. Nat Genet 38: 1397–1405, 2006 [PubMed: 17086182]

7. Brown EJ, Schlöndorff JS, Becker DJ, Tsukaguchi H, Tonna SJ, Uscinski AL, Higgs HN, Henderson JM, Pollak MR: Mutations in the formin gene INF2 cause focal segmental glomerulosclerosis. Nat Genet 42: 72–76, 2010 [PMCID: PMC2980844] [PubMed: 20023659]

8. Mele C, Iatropoulos P, Donadelli R, Calabria A, Maranta R, Cassis P, Buelli S, Tomasoni S, Piras R, Krendel M, Bettoni S, Morigi M, Delledonne M, Pecoraro C, Abbate I, Capobianchi MR, Hildebrandt F, Otto E, Schaefer F, Macciardi F, Ozaltin F, Emre S, Ibsirlioglu T, Benigni A, Remuzzi G, Noris M, PodoNet Consortium : MYO1E mutations and childhood familial focal segmental glomerulosclerosis. N Engl J Med 365: 295–306, 2011 [PMCID: PMC3701523] [PubMed: 21756023]

9. Büscher AK, Konrad M, Nagel M, Witzke O, Kribben A, Hoyer PF, Weber S: Mutations in podocyte genes are a rare cause of primary FSGS associated with ESRD in adult patients. Clin Nephrol 78: 47–53, 2012 [PubMed: 22732337]

10. Suzuki C, Daigo Y, Ishikawa N, Kato T, Hayama S, Ito T, Tsuchiya E, Nakamura Y: ANLN plays a critical role in human lung carcinogenesis through the activation of RHOA and by involvement in the phosphoinositide 3-kinase/AKT pathway. Cancer Res 65: 11314–11325, 2005 [PubMed: 16357138]

11. Watanabe S, Okawa K, Miki T, Sakamoto S, Morinaga T, Segawa K, Arakawa T, Kinoshita M, Ishizaki T, Narumiya S: Rho and anillin-dependent control of mDia2 localization and function in cytokinesis. Mol Biol Cell 21: 3193–3204, 2010 [PMCID: PMC2938385] [PubMed: 20660154]

12. Zhang L, Maddox AS: Anillin. Curr Biol 20: R135–R136, 2010 [PubMed: 20178751]

13. Monzo P, Gauthier NC, Keslair F, Loubat A, Field CM, Le Marchand-Brustel Y, Cormont M: Clues to CD2-associated protein involvement in cytokinesis. Mol Biol Cell 16: 2891–2902, 2005 [PMCID: PMC1142433] [PubMed: 15800069]

14. Collins JS, Schwartz CE: Detecting polymorphisms and mutations in candidate genes. Am J Hum Genet 71: 1251–1252, 2002 [PMCID: PMC385117] [PubMed: 12452182]

15. Sunyaev S, Ramensky V, Koch I, Lathe W, 3rd, Kondrashov AS, Bork P: Prediction of deleterious human alleles. Hum Mol Genet 10: 591–597, 2001 [PubMed: 11230178]

16. Kumar P, Henikoff S, Ng PC: Predicting the effects of coding non-synonymous variants on protein function using the SIFT algorithm. Nat Protoc 4: 1073–1081, 2009 [PubMed: 19561590]

17. Field CM, Alberts BM: Anillin, a contractile ring protein that cycles from the nucleus to the cell cortex. J Cell Biol 131: 165–178, 1995 [PMCID: PMC2120607] [PubMed: 7559773]

18. Ideura H, Hiromura K, Hiramatsu N, Shigehara T, Takeuchi S, Tomioka M, Sakairi T, Yamashita S, Maeshima A, Kaneko Y, Kuroiwa T, Kopp JB, Nojima Y: Angiotensin II provokes podocyte injury in murine model of HIV-associated nephropathy. Am J Physiol Renal Physiol 293: F1214–F1221, 2007 [PubMed: 17652372]

19. Haglund K, Nezis IP, Lemus D, Grabbe C, Wesche J, Liestøl K, Dikic I, Palmer R, Stenmark H: Cindr interacts with anillin to control cytokinesis in Drosophila melanogaster. Curr Biol 20: 944–950, 2010 [PubMed: 20451383]

20. Huber TB, Hartleben B, Kim J, Schmidts M, Schermer B, Keil A, Egger L, Lecha RL, Borner C, Pavenstädt H, Shaw AS, Walz G, Benzing T: Nephrin and CD2AP associate with phosphoinositide 3-OH kinase and stimulate AKT-dependent signaling. Mol Cell Biol 23: 4917–4928, 2003 [PMCID: PMC162232] [PubMed: 12832477]

21. Fackler OT, Grosse R: Cell motility through plasma membrane blebbing. J Cell Biol 181: 879–884, 2008 [PMCID: PMC2426937] [PubMed: 18541702]

22. Akilesh S, Suleiman H, Yu H, Stander MC, Lavin P, Gbadegesin R, Antignac C, Pollak M, Kopp JB, Winn MP, Shaw AS: Arhgap24 inactivates Rac1 in mouse podocytes, and a mutant form is associated with familial focal segmental glomerulosclerosis. J Clin Invest 121: 4127–4137, 2011 [PMCID: PMC3195463] [PubMed: 21911940]

23. Hentschel DM, Mengel M, Boehme L, Liebsch F, Albertin C, Bonventre JV, Haller H, Schiffer M: Rapid screening of glomerular slit diaphragm integrity in larval zebrafish. Am J Physiol Renal Physiol 293: F1746–F1750, 2007 [PubMed: 17699558]

24. Ashworth S, Teng B, Kaufeld J, Miller E, Tossidou I, Englert C, Bollig F, Staggs L, Roberts IS, Park JK, Haller H, Schiffer M: Cofilin-1 inactivation leads to proteinuria—studies in zebrafish, mice and humans. PLoS ONE 5: e12626, 2010 [PMCID: PMC2935884] [PubMed: 20838616]

25. Xie J, Farage E, Sugimoto M, Anand-Apte B: A novel transgenic zebrafish model for blood-brain and blood-retinal barrier development. BMC Dev Biol 10: 76, 2010 [PMCID: PMC2914679] [PubMed: 20653957]

26. Piekny AJ, Glotzer M: Anillin is a scaffold protein that links RhoA, actin, and myosin during cytokinesis. Curr Biol 18: 30–36, 2008 [PubMed: 18158243]

27. Shkreli M, Sarin KY, Pech MF, Papeta N, Chang W, Brockman SA, Cheung P, Lee E, Kuhnert F, Olson JL, Kuo CJ, Gharavi AG, D'Agati VD, Artandi SE: Reversible cell-cycle entry in adult kidney podocytes through regulated control of telomerase and Wnt signaling. Nat Med 18: 111–119, 2012 [PMCID: PMC3272332] [PubMed: 22138751]

28. Oegema K, Savoian MS, Mitchison TJ, Field CM: Functional analysis of a human homologue of the Drosophila actin binding protein anillin suggests a role in cytokinesis. J Cell Biol 150: 539–552, 2000 [PMCID: PMC2175195] [PubMed: 10931866]

29. van Duijn TJ, Anthony EC, Hensbergen PJ, Deelder AM, Hordijk PL: Rac1 recruits the adapter protein CMS/CD2AP to cell-cell contacts. J Biol Chem 285: 20137–20146, 2010 [PMCID: PMC2888426] [PubMed: 20404345]

30. Wei C, Möller CC, Altintas MM, Li J, Schwarz K, Zacchigna S, Xie L, Henger A, Schmid H, Rastaldi MP, Cowan P, Kretzler M, Parrilla R, Bendayan M, Gupta V, Nikolic B, Kalluri R, Carmeliet P, Mundel P, Reiser J: Modification of kidney barrier function by the urokinase receptor. Nat Med 14: 55–63, 2008 [PubMed: 18084301]

31. Ma H, Togawa A, Soda K, Zhang J, Lee S, Ma M, Yu Z, Ardito T, Czyzyk J, Diggs L, Joly D, Hatakeyama S, Kawahara E, Holzman L, Guan JL, Ishibe S: Inhibition of podocyte FAK protects against proteinuria and foot process effacement. J Am Soc Nephrol 21: 1145–1156, 2010 [PMCID: PMC3152231] [PubMed: 20522532]

32. Winn MP, Conlon PJ, Lynn KL, Howell DN, Slotterbeck BD, Smith AH, Graham FL, Bembe M, Quarles LD, Pericak-Vance MA, Vance JM: Linkage of a gene causing familial focal segmental glomerulosclerosis to chromosome 11 and further evidence of genetic heterogeneity. Genomics 58: 113–120, 1999 [PubMed: 10368108]

33. Li H, Durbin R: Fast and accurate short read alignment with Burrows-Wheeler transform. Bioinformatics 25: 1754–1760, 2009 [PMCID: PMC2705234] [PubMed: 19451168]

34. Li H, Handsaker B, Wysoker A, Fennell T, Ruan J, Homer N, Marth G, Abecasis G, Durbin R, 1000 Genome Project Data Processing Subgroup : The Sequence Alignment/Map format and SAMtools. Bioinformatics 25: 2078–2079, 2009 [PMCID: PMC2723002] [PubMed: 19505943]

35. Ge D, Ruzzo EK, Shianna KV, He M, Pelak K, Heinzen EL, Need AC, Cirulli ET, Maia JM, Dickson SP, Zhu M, Singh A, Allen AS, Goldstein DB: SVA: Software for annotating and visualizing sequenced human genomes. Bioinformatics 27: 1998–2000, 2011 [PMCID: PMC3129530] [PubMed: 21624899]

36. Lois C, Hong EJ, Pease S, Brown EJ, Baltimore D: Germline transmission and tissue-specific expression of transgenes delivered by lentiviral vectors. Science 295: 868–872, 2002 [PubMed: 11786607]

37. Westerfield M, The Zebrafish Book: A Guide for the Laboratory Use of Zebrafish (Brachydanio rerio), Eugene, OR, Institute of Neuroscience, 1993

Figures and Tables

Go to:

Figure 1.

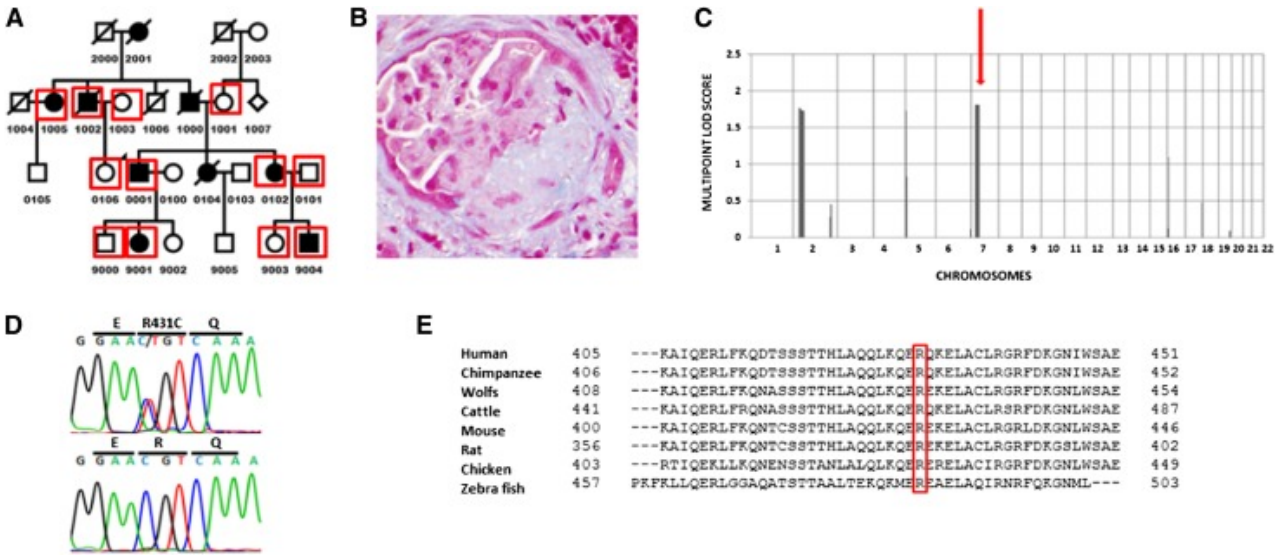

ANLN mutation in a kindred with familial FSGS. (A) Pedigree of a family with familial FSGS. There are at least nine affected family members with male-to-male transmission consistent with an AD mode of transmission. DNA is available from individuals enclosed in red squares and they are genotyped. (B) Representative kidney biopsy histology from an affected individual in family 6562 showing an area of segmental glomerulosclerosis. (C) Genome-wide linkage scan using the Illumina Infinium II HumanLinkage-24 genotyping beadchip assay yields suggestive multipoint LOD scores of 1.7 on chromosomes 2p and 5p and 1.8 on chromosome 7p in family 6562. Chromosome numbers are shown on the *x* axis and LOD scores are on the *y* axis. *ANLN* is located in the chromosome 7p peak (red arrow). (D) Missense heterozygous mutation in exon 7 1291 C>T R431C found in the *ANLN* gene. Top, mutant sequence; bottom, wild-type sequence. (E) The *R431* residue is conserved in evolution to zebrafish (red box).

Table 1.

Clinical characteristics of affected family members

ID	Sex	Genotyped (Yes/No)	Age at Onset (yr)	Proteinuria	Age at ESRD (yr)	Transplant	Recurrence of Disease in Graft
1	Male	Yes	30	Yes	35	Yes	No
102	Female	Yes	30	Yes	40	Yes	No
104	Female	No	Unknown	Unknown	Unknown	Yes	No
1005	Female	Yes	69	Yes	75	No	Unknown
1002	Male		Unknown	Unknown	48	Yes	Unknown
1000	Male	No	Unknown	Unknown	49	Yes	Unknown
2001	Female	No	Unknown	Unknown	36	No	Not applicable
9001	Female	Yes	9	Yes	Unknown	No	Not applicable
9004	Male	Yes	20	Yes	Unknown	No	Not applicable

Table 2.

Novel heterozygous variants in family 6562

Sequencing Approach	Novel Variants (*n*)	Variants after Filtering (*n*)	Variants in the Linkage Region (*n*)	ID of Genes with Variants
Whole exome	1179	146	6	*GCKR* *RASGRP3*[a] *ADCY* *C7ORF31* *ANLN*[a] *NKD2*
Targeted podocyte exome	145	62	2	*RASGRP3*[a] *ANLN*[a]
Variants common to both assays	34	20	2	*RASGRP3* *ANLN*

[a]Genes common to both whole exome and targeted podocyte exome.

Figure 2.

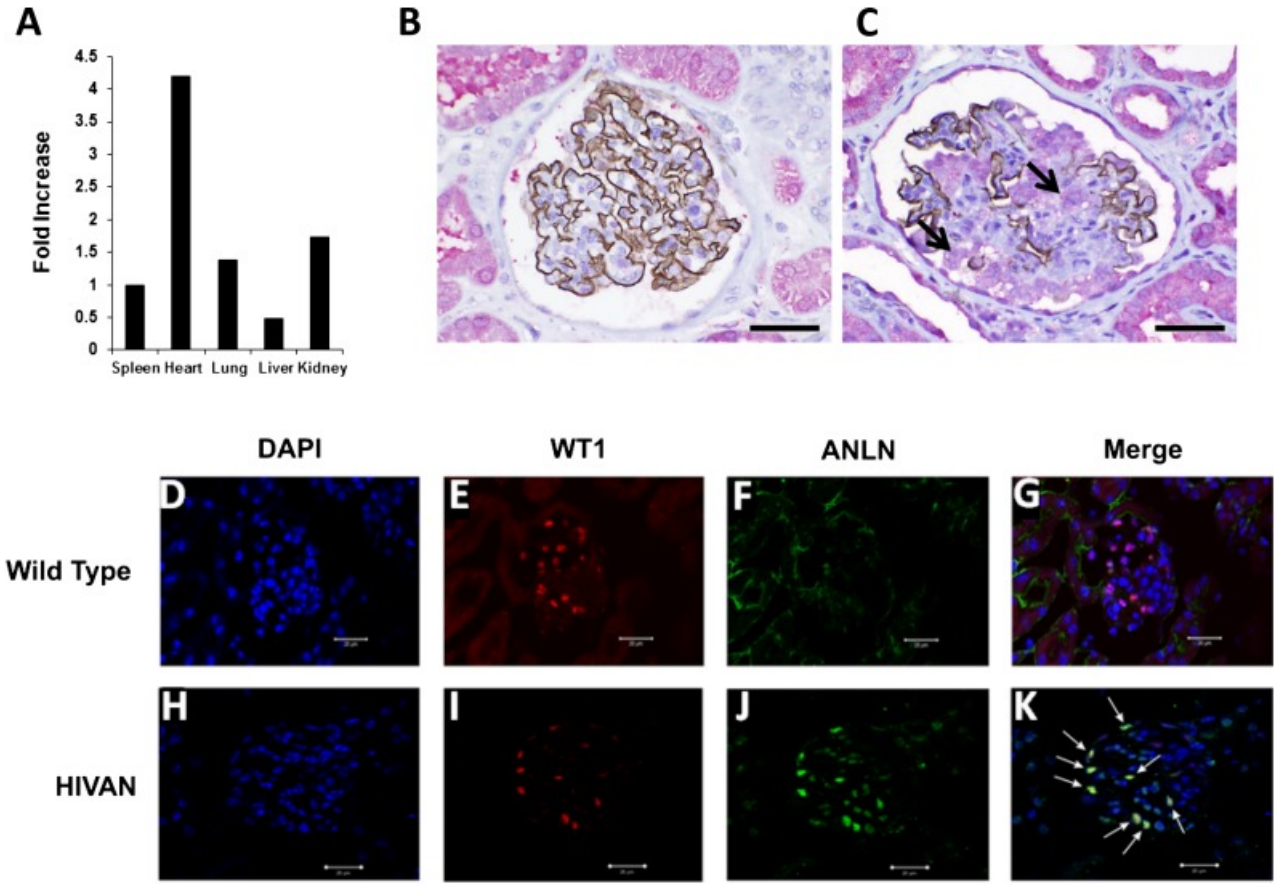

Anillin expression in human and murine FSGS. (A) Real-time PCR is used to assess anillin mRNA expression in different organs. Anillin is ubiquitously expressed in all organs, including the kidney. All values are normalized for expression in the spleen. (B) Normal kidney biopsy tissue is double stained for synaptopodin with anti-human mouse mAb with brown DAB chromogen and anillin anti-human rabbit polyclonal antibody with Fast Red stain. Synaptopodin is strongly expressed in the glomerulus and the podocyte and the expression of anillin is mainly in the tubules. (C) Double staining for synaptopodin and anillin in a glomerulus with FSGS shows patchy expression of synaptopodin in the glomerulus and significant upregulation of anillin expression in the glomerulus and the reactive podocyte (black arrow) compared with normal kidney tissue. (D–G) The middle panel shows double immunostaining for WT1 (red) and anillin (green) in wild-type mice, and DAPI (blue) for nuclear staining. WT1 is expressed in the glomerulus mainly in the nucleus with little or no anillin expression. (I–K) In the lower panel, kidney tissues from HIVAN VPR mice showed reduced expression of WT1 (I), upregulation of anillin in the glomerulus (J), and colocalization of anillin with WT1 (white arrows in K). DAB, diaminobenzidine; DAPI, 4',6-diamidino-2-phenylindole. Original magnification, ×400 in B and C; ×40 in D–K. Scale bars in B and C represent a distance of 50 microns; scale bars in D–K represent a distance of 20 microns.

Figure 3.

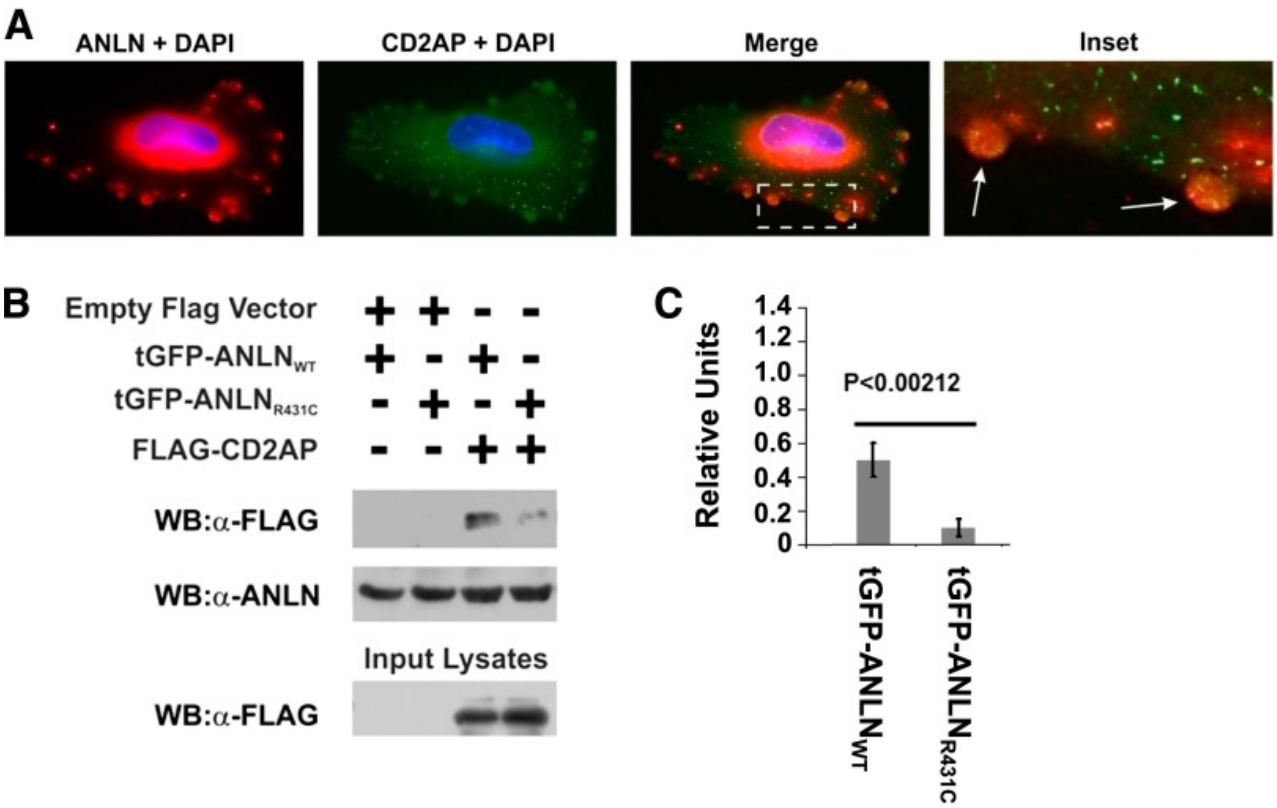

Overexpression of R431C ANLN resulted in aberrant binding to CD2AP. (A) Endogenous anillin protein staining is shown in red. Coimmunolabeling for anti-CD2AP is shown in green. Cell nuclei are stained with DAPI (blue). Anillin is expressed in both the nucleus and cytoplasm of undifferentiated podocyte and colocalizes with CD2AP in plasma membrane blebs. (B and C) $ANLN_{WT}$ and $ANLN_{R431C}$ are coexpressed with flag-tagged CD2AP. After immunoprecipitation with anti-flag antibody, coprecipitation is found with CD2AP. There is significant reduction in binding of the $ANLN_{R431C}$ to CD2AP compared with the $ANLN_{WT}$. The difference is quantified in C. DAPI, 4',6-diamidino-2-phenylindole.

Figure 4.

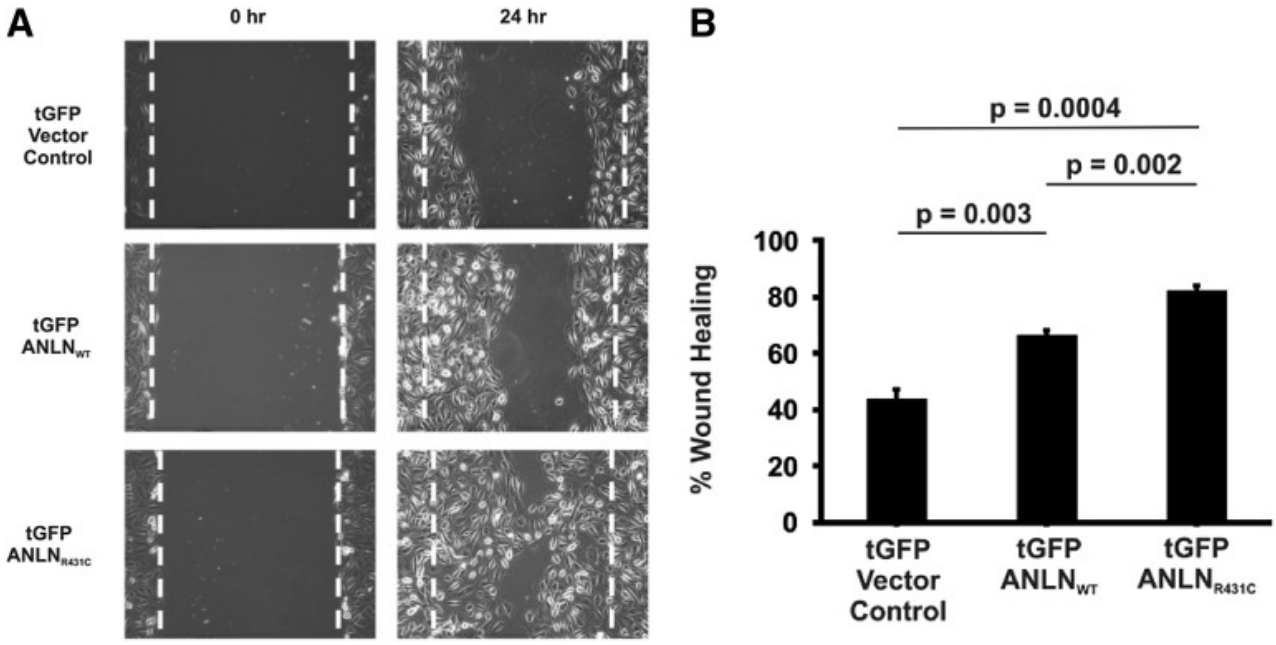

Overexpression of mutant *ANLN* causes aberrant podocyte migration. Immortalized undifferentiated cultured human podocytes are stably transfected with tGFP empty vector control, tGFP-tagged WT ($ANLN_{WT}$), or mutant ($ANLN_{R431C}$) anillin constructs using the lentivirus gene delivery system. (A and B) Motility of the mutant cell line is significantly increased compared with the wild-type overexpression cell line, and both cell lines migrate faster than the tGFP empty vector control cell line.

Figure 5.

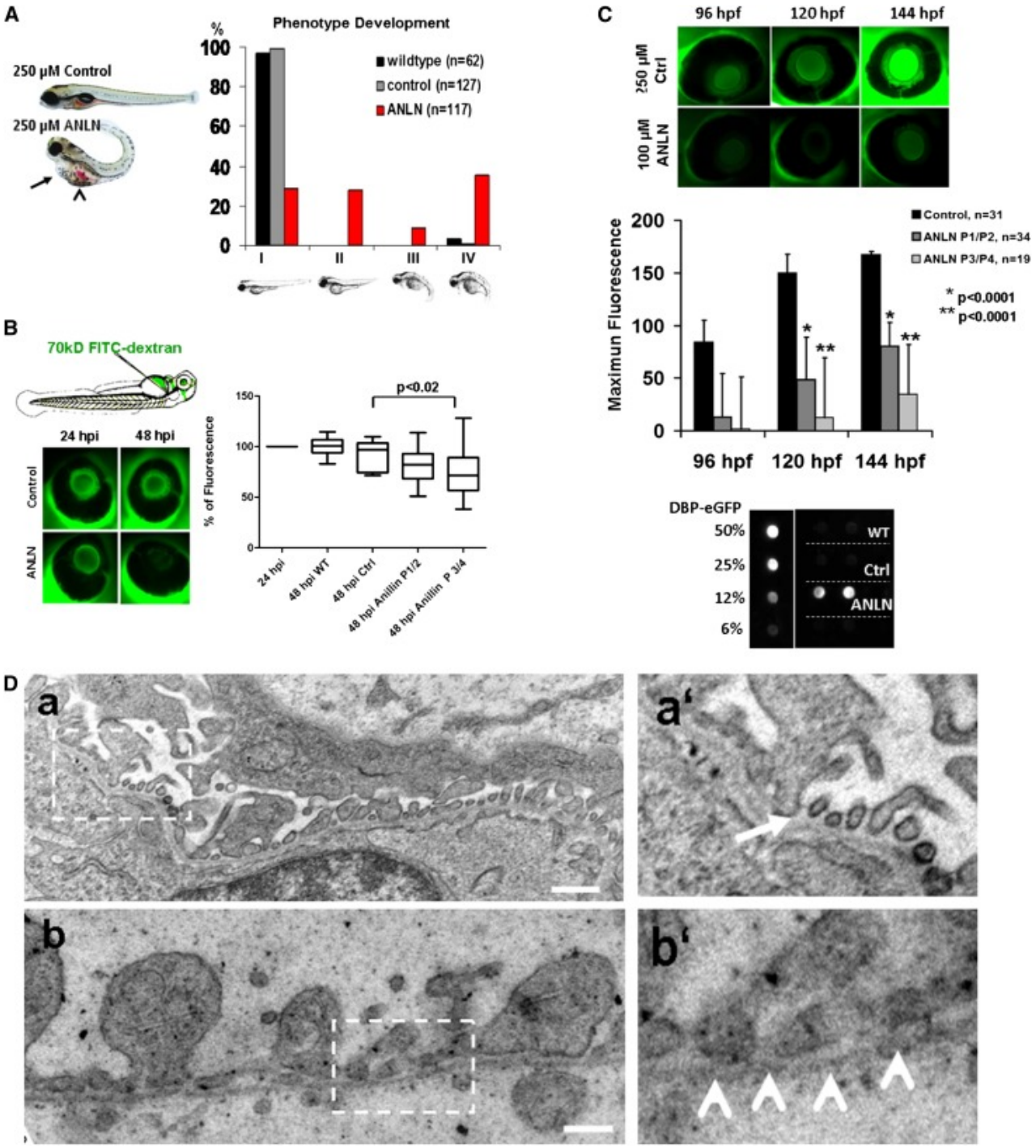

Open in a separate window

Phenotype of anillin knockdown in zebrafish. (A) ANLN knockdown leads to an edema phenotype in zebrafish (pericardial effusion, arrow; yolk sac, arrowhead). Fertilized eggs are injected with a control or Anillin-specific splice-donor morpholino and phenotypes are scored at 120 hours post fertilization (hpf). Edema development is graded as follows: I, no phenotype; II, mild phenotype; III, severe; and IV, very severe phenotype. (B) Anillin-knockdown leads to loss of injected high molecular mass dextran. Zebrafish larvae 48 hpf postinjection of no morpholino (WT), control morpholino (Ctrl), or Anillin morpholino are anesthetized and injected with a FITC-labeled 70-kD dextran. The amount of systemic fluorescence is assessed postinjection by measurement of fluorescence intensity in the retinal blood vessel plexus at baseline and 24 hours later in individual fish. Loss of systemic fluorescence indicates systemic loss of high molecular mass proteins from the circulation, especially in fish with a severe edema phenotype (PIII/PIV). (C) Anillin-

knockdown leads to loss of systemic fluorescence in Tg (l-fabp:DBP-EGFP) zebrafish. Tg (l-fabp:DBP-EGFP) zebrafish develop from 96 hpf until 144 hpf, increasing systemic fluorescence by increasing amounts of circulating EGFP-labeled vitamin D binding protein (molecular mass of approximately 64 kD). Anillin knockdown causes a significant reduction in systemic fluorescence in mild (phenotype I/II) and severely affected (phenotype III/IV) knockdown fish, indicating again systemic loss of high molecular mass proteins. A dot blot assay of DBP-EGFP expression in fish water from anillin-knockdown zebrafish shows strongly detectable fluorescence compared with both control and wild-type fish. (D) TEM of the GFB. In the control morpholino-injected embryo, podocyte foot processes and intervening slit diaphragm architecture are preserved (boxed area in Da and white arrow in Da'). In the anillin-knockdown fish, there is effacement and fusion of the podocyte foot process with disruption of the slit diaphragm (boxed area in Db and white arrow head in Db'). Bar, 500 nm in D.

Articles from Journal of the American Society of Nephrology : JASN are provided here courtesy of **American Society of Nephrology**